A multidisciplinary non-destructive study of historical pipe organ fragments

Daniela Di Martino[a], EnricoPerelli Cippo[b], Winfried Kockelmann[c], Antonella Scherillo[c], Triestino Minniti[c], Roberto Lorenzi[d], Marco Malagodi[e], Curzio Merlo[f], Tommaso Rovetta[e], Giusj Valentina Fichera[e], Michela Albano[e], Zsolt Kasztovszky[g], Ildikó Harsányi[g], Giuseppe Gorini[a]

[a]Dipartimento di Fisica "G. Occhialini", University of Milano-Bicocca, Milan, Italy

[b]Istituto di Fisica del Plasma, CNR, Milan, Italy

[c]STFC, ISIS/RAL Facility, Harwell Campus, Didcot, Oxfordshire, United Kingdom

[d]Dipartimento di Scienza dei Materiali, University of Milano-Bicocca, Milan, Italy

[e]Arvedi Laboratory of Non-Invasive Diagnostics, CISRiC, University of Pavia, Cremona, Italy

[f]Laboratorio di diagnostica applicata ai Beni Culturali, Restoration School – Cr.Forma, Cremona, Italy

[g]Nuclear Analysis and Radiography Dept, Centre for Energy Research, Hungarian Academy of Sciences, Budapest, Hungary

Highlights

• Non-destructive methodology to study bulk tin based metals

• Combination of neutron based techniques and Raman spectroscopy

• Bulk information derived and not only spot details

Abstract

A multidisciplinary non-destructive study has been carried out on historical pipe organ fragments, trying to infer whether the spatial occurrence of different crystallographic phases (that is alpha-tin, beta-tin, cassiterite or romarchite) reflects the visible alterations patterns. We could indeed derive the presence of the beta-tin phase. Several tin oxide phases have been detected too, associated with the visible occurrence of "grey regions" and hole borders (mapped by Raman spectroscopy), and hydrate phases (mapped by neutron imaging).

We aim to demonstrate that neutron and Raman techniques can give relevant indications in archaeometallurgy studies of cultural heritage artifacts, where only non-destructive experiments can be performed. The combination of the two probes could be considered a protocol to be applied in the characterization of tin based specimens.

Keywords: Neutron based non-destructive testing; Raman spectroscopy; Tin pest; Archaeometallurgy

1. Introduction

Organs are very sophisticated and majestic musical instruments, also thanks to the power and timbre of the sound they produce. Organ pipes are often made of metals, but each metal alloy clearly influences the characteristics of the sound resulting from the pipe. Lead and tin alloys were the most used materials for historical pipes. Thanks to their shine, tin pipes were mostly used for the instruments façade, but had a severe draw-back, the so-called tin pest [1]. Tin pest is indeed an autocatalytic allotropic transformation of tin, from the ductile metallic β-phase (white tin) to the brittle, nonmetallic, α-phase [2,3]. This phase transformation is spontaneous at temperatures of 13.2 °C and below, but it is strongly accelerated by lower temperatures (roughly below −30 °C [1]), highly humid atmosphere or high concentration of halides in the environment (for instance in seaside towns) [4]. On the other hand, the addition of lead, antimony or other metals to the cast would usually delay the process [2]. Due to the paramount relevance of pipe organs in European musical tradition, the importance of restoration and early diagnosis of the degradation processes of metal pipes is evident. The characterization of the metal alloy used for the pipe is of great importance for the conservation of historical pipes. Several studies were devoted to this topic [2,[4], [5], [6], [7]], but the degradation of tin-based organs pipes has still many open questions.

We studied a set of fragments coming from selected Italian historical organs pipes. Preliminary examinations involved techniques such as stereomicroscopy, X-ray fluorescence spectroscopy (XRF) and Scanning Electron Microscopy with Energy-Dispersive X-ray spectroscopy (SEM-EDX) [8]. We further investigated two of the samples by non-destructive neutron techniques like neutron diffraction (ND), neutron imaging (NI) and prompt-gamma activation analysis (PGAA), gathering essential information on the composition of the bulk of the samples and revealing beta-tin phase and tin oxides, but no alpha-tin phase. Finally, a Raman study was also carried out to map the areas where tin oxides are present. Our multidisciplinary study tried to infer whether the spatial occurrence of different crystallographic phases (that is alpha-tin, beta-tin, or other tin oxides like cassiterite or romarchite) reflects the visible alterations patterns. Moreover, we tried to better clarify the degradation processes, and to show how non-destructive examinations could be of benefit for restoration and conservation of historical pipe organs. This protocol could be applied to the study of several other metallic (tin based) items, with the major benefit of returning bulk information (and not only spot details) in a non-destructive way.

Neutron techniques were seldom applied to the analysis of organ pipes. Only a previous PGAA study was found in the literature, concerning organ reed pipes [9]. On the contrary, other kinds of techniques like analysis by differential scanning calorimetry-differential thermal analysis (DSC-DTA), metallographic and SEM analysis were used to study the crystallographic phases of Italian tin-based organ pipes of different ages [6,7]. However, all these techniques are destructive for the investigated samples, and can only be used in selected cases.

2. Materials and Methods

2.1. Samples

The samples under investigation are shown in Fig. 1. They are fragments of a tin-rich alloy organ pipe (mid-eighteenth century), coming from an instrument placed in the church of San Giovanni Battista in Chieti (Abruzzo) in central Italy. The organ builder is known as Francesco Pasquale d'Onofrio da Caccavone. The fragments come from the same pipe.

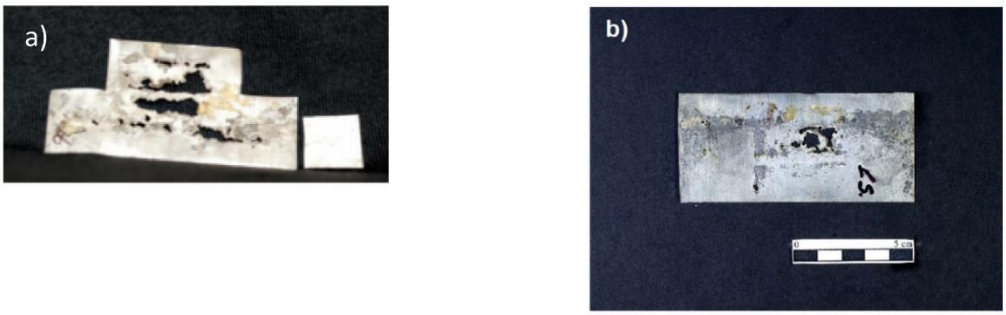

Fig. 1. Some organ pipe fragments made available for the present investigation (A sample on the left and B sample on the right, coming from the same pipe and with similar sizes). In both specimens tin pest at various stages is clearly visible.

2.2. Experimental Techniques

Time of Flight (ToF) neutron diffraction (ND) experiments were run at the Italian Neutron Experimental Station (INES) of the ISIS spallation neutron source (UK), the ToF technique being a general method for determining the kinetic energy of a neutron, by measuring the time it takes to travel between neutron source and detector the distance of which is known. The INES beamline is designed and optimized for archaeometric measurements [10], where non-destructive studies in archaeometallurgy were conducted recently [[11], [12], [13], [14]]. ND was carried out also on the General Materials Diffractometer GEM at ISIS [15]. The ND data were processed using the Mantid software [16], for data normalization, detector efficiency correction and for conversion to diffraction patterns, which were then analyzed with LeBail and Rietveld refinement techniques using the GSAS (General Structure Analysis System) code [17] with the EXPGUI interface [18]. By using this procedure, the weight percentages of the identified phases can be quantitatively determined.

PGAA was carried out at the Budapest Neutron Centre (BNC, Budapest, Hungary), at the NIPS-NORMA instrument on a horizontal cold neutron beamline [19]. The PGAA method is based on the detection of prompt- and delayed γ-photons produced in nuclear reactions induced by neutrons. The photon energies are characteristic for the emitting nuclei, while the numbers of the photons are proportional to the amount of the given element in the sample. Thus, the method is quantitative [20]. The calculation of element concentrations is based on the k0-method [21].

Neutron imaging (NI) measurements, both in white beam and energy resolved mode, were run at IMAT (ISIS) [22]. When neutrons are transmitted though materials, the universal law of attenuation of radiation passing through matter (Beer-Lambert law) is valid. IMAT offers also energy resolved NI, studying energy-dependences of neutron attenuation in several-mm thick samples by Bragg edge analysis. This could allow in principle to determine spatial distributions of tin phases. The neutron counting detector, based on a stack of Microchannel Plates (MCPs), has a Field-of-View (FoV) of $28 \times 28\ mm^2$ and 55 µm of spatial resolution [23].

Micro-Raman measurements were carried out at room temperature by a confocal labRAM (Horiba Jobin-Yvon) spectrometer, operating in backscattering configuration with a focal layer thickness of few microns. A helium–neon laser line at 632.8 nm was used as exciting source with spectral resolution of about 2 cm−1. The scattered light was detected by a charge coupled device (CCD-Sincerity, JobinYvon). A microscope (Olympus BX40) was used to focus the excitation on the samples and to collect the scattered radiation, by three different objectives 20× with numerical apertures (NA) of 0.40, 50× (NA = 0.75) and 100× (NA = 0.95),

with resulting sampled areas of ~10, 5 and 2 μm diameter, respectively, and a laser power on the sample of <10 mW. The sampled area could be selected after inspection of the sample surface, illuminated by an optical fiber and by using a camera.

3. Results and Discussion

Samples A and B show clear indications of alterations, like holes and grey regions (dark and light grey areas, with pustules too – see Fig. 1). In order to identify the metal alloy used for the pipe, to assess incipient degradation phenomena and to prevent further degradation, we tried to disclose: (i) elemental composition (by PGAA), (ii) phase composition (by ToF-ND), and spatial occurrence of different phases by NI and Raman techniques.

PGAA results on sample B are listed in Table 1, giving the composition by major and minor components (as weight percent, with their absolute uncertainties). We can derive that the main component is tin; in addition, other minor components are present and could influence the tin phase transformation [2].

Table 1. PGAA results, with percentage errors (see text for details).

Sample B (Code AY23_REPB9)	
Element	**wt% (percentage error)**
Sn	99.0 ± 0.1%
Cu	0.37 ± 0.01%
Fe	0.07 ± 0.005%
Pb	0.5 ± 0.09%
Cl	0.0158 ± 0.0005%
B	0.000052 ± 0.000002%

We underline that the PGAA method is, in principle, sensitive for every chemical element and even isotopes of the same element. However, due to the different neutron absorption cross-sections for different nuclei, not every minor (or trace) elements could be detected. Moreover, since neutrons easily cross all the sample thickness of several millimetres, through the inspected area determined by the cross-section of the beam, the results are representative for the whole irradiated volume, and can be considered bulk results.

By ND, we tried to infer the crystallographic phases. Diffraction data were collected on A and B samples. At first a test at INES was carried out on sample A, and then a further diffractogram was collected on GEM on sample B. The results can be compared, since both specimens are coming from the same organ pipe. In Fig. 2 the fitted diffractograms are displayed. In particular, two different types of fits were applied: LeBail and Rietveld full pattern refinements. By LeBail, beta-tin fits all the large peaks, while by Rietveld we can derive, besides the beta-tin phase, <1% cassiterite and no romarchite, and <0.5% of Pb. There is at least one other non-identified phase (d-spacings: 2.47 and 2.56 Å) and strong texture (not included in the Rietveld model). No signal related to the alpha-tin phase was detected.

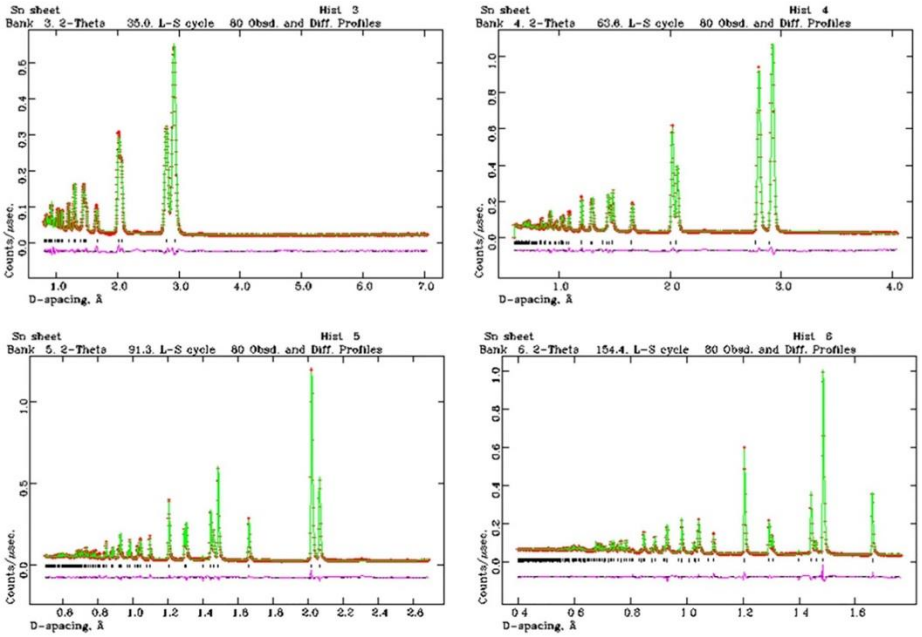

Fig. 2. Neutron diffraction patterns on sample B, collected on GEM.

In order to determine the spatial distribution of the tin phases and the energy-dependences of neutron attenuation, we used imaging techniques on IMAT. The results, both in white beam and energy-dispersive neutron imaging are shown in Fig. 3. A cadmium marker is clearly evident, returning the maximum neutron attenuation. Regions showing the darkest greyscale are thus parts containing elements with high neutron attenuation. We could indeed easily distinguish by neutron imaging some voids (that are regions with the lowest neutron attenuation, so very light in greyscale) and corrosion points (where on the opposite we have a higher neutron attenuation). In fact, the darkest regions are likely connected to H-bearing phases, though preliminary measurements did not detect any hydrate phases. Thanks to the energy selective mode, we tried to select Bragg edges in the Region of Interest (ROI). The transmission profiles in different ROI are shown in Fig. 3. Unfortunately, we could not derive any spatial (thickness) distribution of the beta-tin phase, nor identify the alpha-tin phase: the sample was too thin to return a tin phase mapping. Moreover, the presence of craters and pustules were already studied by SEM-EDX, pointing out only a substantial reduction of Pb on the alteration edges (9.57–0.54%) [8].

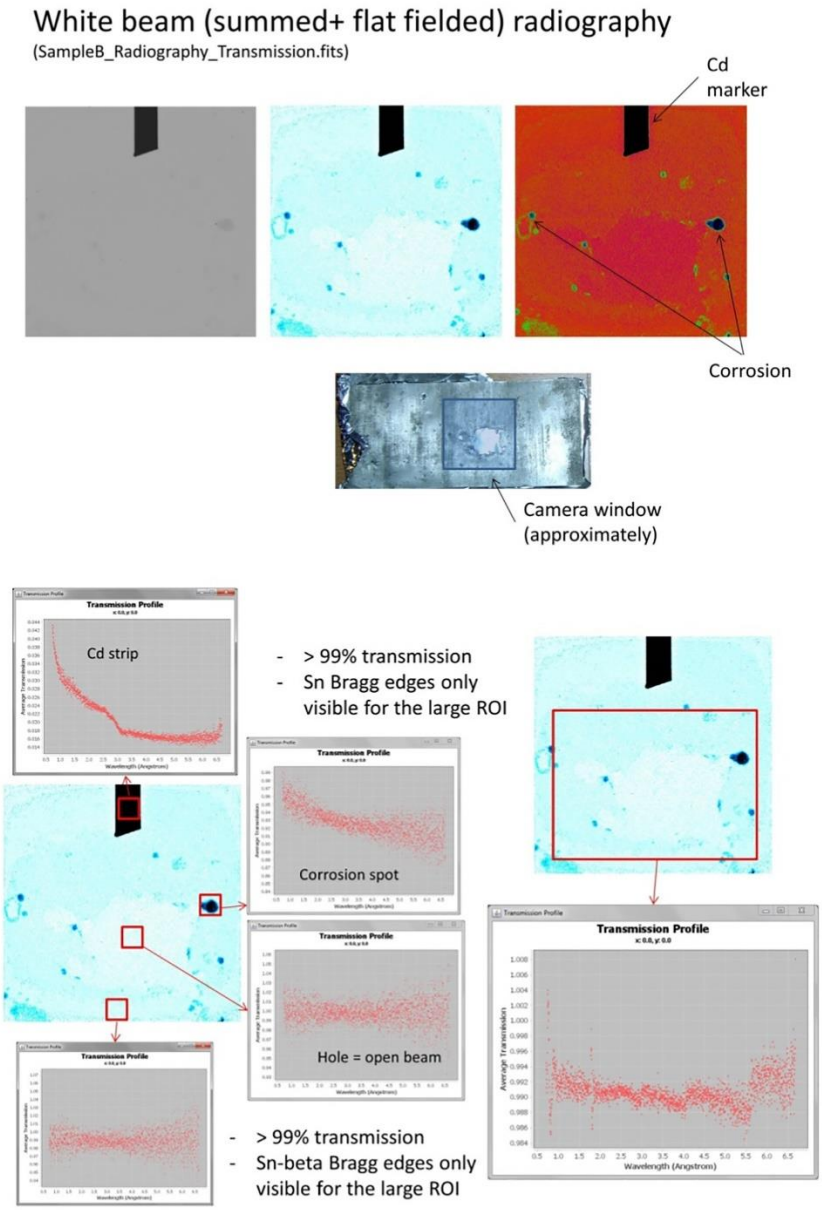

Fig. 3. White beam (top) and energy-dispersive (bottom) neutron imaging on sample B. See text for details.

Finally, Raman spectra on different points of sample A were collected and a line mapping was recorded with the occurrence of different tin oxides (pure tin is not detectable). The results are displayed in Fig. 4 and summarized in Table 2. The main Raman spectra representative of the different phases present in the sample are reported in Fig. 4b together with reference spectra from the literature. In particular, all the spectra are ascribable to tin oxides (SnOx, $1 < x < 2$) and hydroxides. A spectrum collected in point A shows a sharp strong peak at 168 cm−1 and a larger peak at 622 cm−1 with satellites in the range 400–800 cm−1. The first strong peak is relative to partial oxidation of Sn to Sn3O4 phase [[24], [25], [26]] and has been found also in point B and, as a minor component, in point D. The spectral features in the region 400–800 cm−1 are ascribable to SnO2 in the cassiterite phase [27]. The main peak is at 622 cm−1, with a full width at half maximum (FWHM) of about 30 cm−1 corresponding to the A1g mode. These values are slightly different with respect to the reported literature values for SnO2 single crystal with the peak centered at 634 cm−1 and a FWHM of 10 cm−1 (RRUFF R040072, [28]). Nevertheless, both the peak shifts to lower wavenumbers, as well as broadening have reported for SnO2 with poor crystalline features such as in cassiterite nanoparticle, thin films and amorphous SnO2 [[29], [30], [31]]. Moreover, the incorporation of

heavier and smaller ions substitutional of tin atoms, such as lead, further lowers the characteristic frequency [32,33]. As already mentioned, the spectrum collected in point B shows a sharp peak at 167 cm−1 distinctive of Sn3O4. A second broader peak at 206 cm−1 can be found also in points C and D – corresponding to a dark grey pustule – and it is related to the presence of the main oxide found in our Raman analysis, that is the SnO in the romarchite phase ([26,34], RRUFF R080006 [28]). Finally, the presence of a second peak at 226 cm−1 registered on point C implies further oxidative processes leading to the hydroxylation of romarchite to hydroromarchite Sn3O2(OH)2 ([34], RRUFF: R090060 [28]).

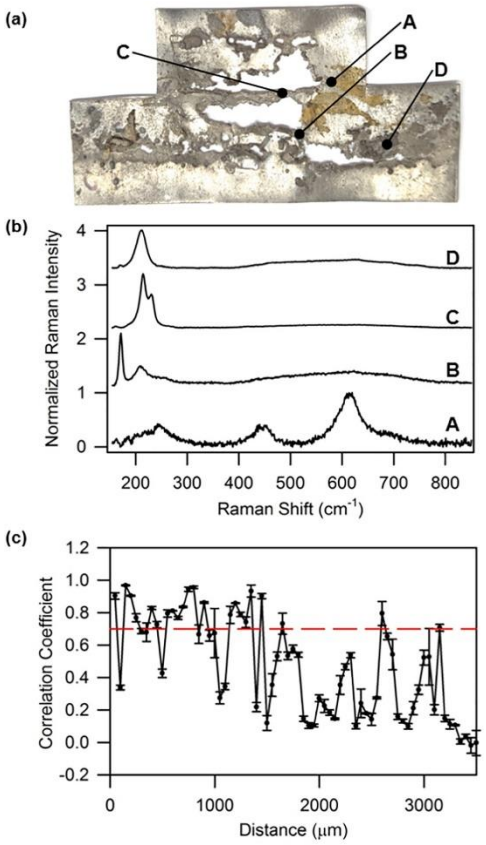

Fig. 4. (a) Photograph of sample A with indication of spots where Raman spectra were recorded. (b) Representative Raman spectra of the different active phases found in the studied organ pipe, labels refer to (a). (c) Pearson's correlation coefficient map of romarchite with respect to spectra collected longitudinal to the corrosion profile indicated by C in (a); the dashed line (in red in the online version) indicates a coefficient of 0.7 representative of reliable correlation.

Table 2. Peak position of the main phases found in Raman spectra collected in this work and comparison with literature data.

Point	Phase	Raman shift (cm^{-1})	
		This work	Literature
A	Sn_3O_4	168	170 [25]
	SnO_2	622	634 [28] (RRUFF: R040072)
B	Sn_3O_4	167	170 [25]
	SnO	206	203 [28] (RRUFF: R080006)
C	SnO	208	203 [28] (RRUFF: R080006)
	$Sn_3O_2(OH)_2$	226	226 [28] (RRUFF: R090060)
D	SnO	206	203 [28] (RRUFF: R080006)

To quantify the corrosion extent, we performed line mapping in correspondence of point C. Data have been analyzed according to Principal Component Analysis [35]. The most important phases collected in the corroded area pertain to both romarchite and hydroromarchite. Fig. 4c reports the line profile of the Pearson's correlation coefficient, with values comprised between spectra collected along the line and the reference spectrum of romarchite which is the principal phase of the corroded area, with values comprised between 1 (complete correlation) and −1 (complete anti-correlation), while 0 indicates absence of correlation. As a reliable index of correlation we can assume a value of 0.7, i.e. correlation coefficients higher than 0.7 indicate the presence of the romarchite phase. As can be seen by the line mapping, the oxidative processes proceed about 1.5 mm from the hole to the interior of the deteriorated area. The presence of H-bearing phase is in agreement with our NI imaging results.

4. Conclusions

A multidisciplinary characterization of pipe organ fragments has been carried out, aiming at a bulk material characterization mainly in the altered regions. By neutron diffraction we could indeed derive, in a complete non-destructive way, the presence of beta-tin phase. Several tin oxide phases were revealed, but no alpha-tin phase was detected. We could associate them with the visible occurrence of “grey regions”, in the degraded parts, with a preference for the romarchite phase at the surface of the borders of holes. Hydrate phases are also present, clearly mapped by neutron imaging. The detection of oxidative phases is important for an archeometallurgical characterization and for conservative issues, since these phases could be in principle treated. A similar multidisciplinary protocol, able to study the whole sample and not only based on spot measurements, could be applied to the study of several other metallic (tin based) items, with the benefit of being non-destructive. In the case of archaeological artifacts this could be mandatory, and the results could guide restorers and conservators in their practices.

Acknowledgments

The authors would like to gratefully acknowledge Claudio Bonizzi for providing samples of organ pipes and for his precious technical information. This work was supported within the CNR-STFC Agreement 2014–2020, concerning collaboration in scientific research at the spallation neutron source ISIS (UK). Financial support by the Access to Research Infrastructures activity in the Horizon 2020 Programme of the EU

(IPERION CH Grant Agreement n. 654028) is gratefully acknowledged (FIXLAB: Budapest Neutron Centre, Hungary). Finally, the authors thank the anonymous reviewers for their valuable comments which helped to improve the manuscript.

[1] C.E. Homer, H.C. Watkins
Transformation of tin at low temperatures
The Metal Industry (London) (1942)
(LX 22)

[2] C. Chiavari, C. Martini, G. Poli, D. Prandstraller
Deterioration of tin-rich organ pipes
J. Mater. Sci., 41 (2006), pp. 1819-1826, 10.1007/s10853-006-2896-0

[3] ASM International and The Dialog Corporation
Alloy phase diagrams
ASM Handbook on CD-ROM, vol. 3 (1999)

[4] A. Bovelacci, E. Ciliberto, E. Greco, E. Viscuso
Surface and bulk investigations of organ metal pipe degradation
Proc. Chem., 8 (2013), pp. 130-138, 10.1016/j.proche.2013.03018

[5] C. Chiavari, et al.
Atmospheric corrosion of historical organ pipes: the influence of environment and materials
Corros. Sci., 50 (2008), pp. 2444-2455

[6] C. Mapelli, W. Nicodemi, R. Venturini
Analysis and research of damage phenomena on tin based organ pipes of different ages
Surf. Eng., 21 (2005), pp. 373-377

[7] C. Mapelli, W. Nicodemi, R. Venturini
Characterization of damaging phenomena interesting tin-based organ pipes of different ages
Rev. Metall. Cah. Inf. Tech., 102 (2005), p. 153

[8] M. Albano, et al.
Microstructural investigations on historical organ pipes
J. Mater. Sci., 52 (2017), pp. 9859-9871, 10.1007/s10853-017-1134-2

[9] A. Manescu, et al.
Non-destructive compositional analysis of historic organ reed pipes
J. Phys. Condens. Matter, 20 (2008), Article 104250

[10] S. Imberti, et al.
Neutron diffractometer INES for quantitative phase analysis of archaeological objects
Meas. Sci. Technol., 19 (2008), Article 034003

[11] D. Di Martino, et al.
Disclosing mineralogical phases in medioeval iron nails by non-destructive neutron techniques
Archaeol. Anthropol. Sci., 9 (2017), pp. 515-522

[12] A. Fedrigo, et al.
Extraction of archaeological information from metallic artefacts—a neutron diffraction study on Viking swords
J. Archaeol. Sci. Rep., 12 (2017), pp. 425-436, 10.1016/j.jasrep.2017.02.014

[13] J. Corsi, et al.
Compositional and microstructural characterization of Celtic silver coins from northern Italy using neutron diffraction analysis
Microchem. J., 126 (2016), pp. 501-508, 10.1016/j.microc.2016.01.006

[14] F. Grazzi, et al.
Determination of the manufacturing methods of Indian swords through neutron diffraction
Microchem. J., 125 (2016), pp. 273-278, 10.1016/j.microc.2015.11.035

[15] A.C. Hannon
Results on disordered materials from the GEneral Materials diffractometer, GEM, at ISIS
Nucl. Instrum. Methods Phys. Res. Sect. A, 551 (2005), pp. 88-107

[16] O. Arnold, et al.
Mantid—data analysis and visualization package for neutron scattering and μSR experiments
Nucl. Instrum. Methods Phys. Res. Sect. A, 764 (2014), pp. 156-166

[17] A.C. Larson, R.B. Von Dreele
General Structure Analysis System (GSAS), Los Alamos National Laboratory Report, LAUR
(2004), pp. 86-748

[18] B.H. Toby
EXPGUI, a graphical user interface for GSAS
J. Appl. Crystallogr., 34 (2001), pp. 210-213

[19] Z. Kis, L. Szentmiklósi, T. Belgya
NIPS–NORMA station - a combined facility for neutron-based nondestructive element analysis and imaging at the Budapest Neutron Centre
Nucl. Instr. Methods A, 779 (2015), pp. 116-123

[20] Zs. Révay, T. Belgya
Principles of the PGAA method
G.L. Molnár (Ed.), Handbook of Prompt Gamma Activation Analysis, Kluwer Academic Publishers (2004), pp. 1-30

[21] Zs. Révay
Determining elemental composition using prompt gamma activation analysis

Anal. Chem., 81 (2009), pp. 6851-6859

[22] T. Minniti, et al.
Characterization of the new neutron imaging and materials science facility IMAT
Nucl. Instr. Method A, 888 (2018), pp. 184-195

[23] A.S. Tremsin
Detection efficiency, spatial and timing resolution of thermal and cold neutron counting MCP detectors
Nucl. Instr. Method A, 604 (10) (2009)

[24] H. Song, S.-Y. Son, S.K. Kim, G.Y. Jung
A facile synthesis of hierarchical Sn3O4 nanostructures in an acidic aqueous solution and their strong visible-light-driven photocatalytic activity
Nano Res., 8 (2015), pp. 3553-3561

[25] Y. He, D. Li, J. Chen, Y. Shao, J. Xian, X. Zheng, P. Wang
Sn3O4: a novel heterovalent-tin photocatalyst with hierarchical 3D nanostructures under visible light
RSC Adv., 4 (2014), pp. 1266-1269

[26] J. Geurts, S. Rau, W. Richter, F. Schmitte
SnO films and their oxidation to SnO2: Raman scattering, IR reflectivity and X-ray diffraction studies
Thin Solid Films, 121 (1984), pp. 217-225

[27] J.F. Scott
Raman spectrum of SnO2
J. Chem. Phys., 53 (1970), pp. 852-853

[28] B. Lafuente, R. Downs, H. Yang, N. Stone, T. Armbruster, R. Danisi
Highlights in Mineralogical Crystallography
W. De Gruyter, Berlin (2015), pp. 1-30

[29] F. Aragón, J. Coaquira, P. Hidalgo, S. da Silva, S. Brito, D. Gouvêa, P. Morais
Evidences of the evolution from solid solution to surface segregation in Ni-doped SnO2 nanoparticles using Raman spectroscopy
J. Raman Spectrosc., 42 (2011), pp. 1081-1086

[30] A. Dieguez, A. Romano-Rodrıguez, A. Vila, J. Morante
The complete Raman spectrum of nanometric SnO2 particles
J. Appl. Phys., 90 (2001), pp. 1550-1557

[31] S. Mehraj, M.S. Ansari
Annealed SnO2 thin films: structural, electrical and their magnetic properties
Thin Solid Films, 589 (2015), pp. 57-65

[32] S. Sarangi, G.K. Pradhan, D. Samal
Band gap engineering in SnO2 by Pb doping

J. Alloys Compd., 762 (2018), pp. 16-20

[33] B. Mallesham, P. Sudarsanam, G. Raju, B.M. Reddy
Design of highly efficient Mo and W-promoted SnO2 solid acids for heterogeneous catalysis: acetalization of bio-glycerol
Green Chem., 15 (2013), pp. 478-489

[34] M. Chen, X. Grandbois
In situ Raman spectroscopic observation of sequential hydrolysis of stannous chloride to abhurite, hydroromarchite, and romarchite
J. Raman Spectrosc., 44 (2013), pp. 501-506

[35] A.K. Shinzawa Hideyuki, et al.
Multivariate data analysis for Raman spectroscopic imaging
J. Raman Spectrosc., 40 (2009), pp. 1720-1725